# Incorporating uncertainty of future sea-level rise estimates into vulnerability assessment: A case study in Kahului, Maui

Hannah M. Cooper · Qi Chen

**Abstract** Accurate sea-level rise (SLR) vulnerability assessments are essential in developing effective management strategies for coastal systems at risk. In this study, we evaluate the effect of combining vertical uncertainties in Light Detection and Ranging (LiDAR) elevation data, datum transformation and future SLR estimates on estimating potential land area and land cover loss, and whether including uncertainty in future SLR estimates has implications for adaptation decisions in Kahului, Maui. Monte Carlo simulation is used to propagate probability distributions through our inundation model, and the output probability surfaces are generalized as areas of high and low probability of inundation. Our results show that considering uncertainty in just LiDAR and transformation overestimates vulnerable land area by about 3 % for the high probability threshold, resulting in conservative adaptation decisions, and underestimates vulnerable land area by about 14 % for the low probability threshold, resulting in less reliable adaptation decisions for Kahului. Not considering uncertainty in future SLR estimates in addition to LiDAR and transformation has variable effect on SLR adaptation decisions depending on the land cover category and how the high and low probability thresholds are defined. Monte Carlo simulation is a valuable approach to SLR vulnerability assessments because errors are not required to follow a Gaussian distribution.

## 1 Introduction

Natural and human coastal systems with low elevations are most vulnerable to global sea-level rise (SLR). The causes of SLR are due to the physical processes of thermal expansion of ocean waters, and the release of land-based ice into the ocean (Meehl et al. 2007). Average global sea level is rising at a current rate of 3.2±0.4 mm/year (Church and White 2011). Accelerated SLR complicates natural and human coastal systems' ability to adapt (Schaeffer et al. 2012). Consequently, accurate SLR vulnerability assessments are of great significance to better prepare vulnerable coastal systems for rising seas (U.S. Climate Change Science Program 2009; Gesch 2009).

H. M. Cooper (✉) · Q. Chen
Department of Geography, University of Hawai'i, 2424 Maile Way, Honolulu, HI 96822, USA
e-mail: hcooper2013@fau.edu

Q. Chen
e-mail: qichen@hawaii.edu

Uncertainty is just as important as the SLR vulnerability assessments that are useful for coastal managers and scientists. SLR vulnerability assessments are more reliable when they account for uncertainty (Purvis et al. 2008; Gesch 2009; Gesch 2013). Although it is difficult to quantify some uncertainties such as future coastal development and infrastructure, it is easy to quantify elevation uncertainties in Light Detection and Ranging (LiDAR), any offsets between tidal and orthometric datums and datum transformations. In order to make informed decisions based on these support tools, it is better to consider quantifiable sources of uncertainties in SLR vulnerability assessments.

LiDAR Digital Elevation Models (DEMs) are more often being used as the principal data layer in SLR vulnerability assessment (e.g., Poulter and Halpin 2008; Zhang 2011). The uncertainty in LiDAR is sometimes quantified as the standard deviation ($\sigma$), but most commonly, LiDAR error is calculated using National Standard for Spatial Data Accuracy (NSSDA; FGDC 1998) procedures for the Root Mean Square Error (RMSE) and linear error at the 95 % confidence interval. It is important to note that the NSSDA linear error is based on the assumptions that: 1) errors follow a Gaussian distribution, and 2) the elevation data has a zero bias so that the RMSE may be used in place of the standard deviation ($\sigma$) (Cooper et al. 2013). This is important for the following approaches that consider error in SLR vulnerability assessment. LiDAR error is addressed where the NSSDA linear error is mapped above (Gesch 2009) and below (Gesch 2012; Gesch 2013) the inundation extent. Building on this approach, Gesch (2013) combines LiDAR RMSE with local water levels and transformation among tidal datums (quantified as $\sigma$ in NOAA's VDatum estimates; National Oceanic and Atmospheric Administration NOAA 2012) using summing in quadrature. The approach by National Oceanic Atmospheric Administration (NOAA) (2010), also implemented by Mitsova et al. (2012), takes into account the LiDAR RMSE and offset between tidal and orthometric datums quantified as $\sigma$ and 'assumes that the RMSE is analogous to the $\sigma$ (i.e. the data are not biased), which allows for the generation for a type of z-score or "standard score" from the data' (National Oceanic Atmospheric Administration NOAA 2010: 3). However, sometimes LiDAR are biased limiting these approaches that require all uncertainties to follow a Gaussian distribution with zero bias (Cooper et al. 2013).

Assessing SLR vulnerability calls for an additional approach that does not require all uncertainties to follow a Gaussian distribution with zero bias. Future SLR estimates constitute another important source of uncertainty that is often overlooked. This may be because it is not common practice to complete a formal probability analysis on SLR projections. This has led to the approach by Purvis et al. (2008) to formalizing the unknown real distribution (e.g. whether Gaussian, non-Gaussian, uniform, etc.) of SLR estimates in terms of a triangular distribution. A Monte Carlo approach would allow for the consideration of SLR estimates formalized as a triangular distribution in addition to LiDAR that follow a non-Gaussian distribution. Monte Carlo is a technique to propagating distributions by random sampling from probability distributions, which is useful when uncertainties depart from a Gaussian distribution or scaled and shifted t-distribution (JCGM and Joint Committee for Guides in Metrology 2008). Therefore, Monte Carlo simulation is a valuable approach to SLR vulnerability mapping because errors are not required to follow a Gaussian distribution.

The purpose of this study is threefold: 1) to extend the approach by National Oceanic Atmospheric Administration (NOAA) (2010) to Monte Carlo simulation so that we may include uncertainty in future SLR estimates, 2) evaluate the effect of combining uncertainties in LiDAR, transformation and future SLR estimates on estimating potential land area and land cover loss, and 3) examine whether including uncertainty in future SLR has implications for adaptation decisions in Kahului, Maui. The following section introduces the study area and LiDAR data. Section III presents methods to calculate local water levels and transform the

LiDAR DEM between vertical datums, formalizing future SLR estimates as a probability distribution, and probability inundation modeling. Section IV reports results and discussion. The final section V presents conclusion and areas for future research.

## 2 Study area and LiDAR data

### 2.1 Study area

The study area (8.7 km$^2$) of Kahului is located in a low-relief isthmus along the north central shore of the Island of Maui, Hawaiʻi, and is between two shield volcanoes: the extinct West Maui volcano and dormant Haleakalā volcano to the east (Fig. 1). Two parks serve as a favorite destination for locals: (1) Kahului Harbor Park for the fishing pier and wave quality, and (2) Kanaha Beach Park for kiteboarding and windsurfing due to the funneling effect produced by the northeast trade winds blowing between the West Maui and Haleakalā volcanoes. Since Kahului is the largest community in Maui with a Census 2010 population of nearly 26,000, it also serves as the Island's industrial, commercial, and urban centers. Adjacent to the Central Maui Wastewater Facility and Kahului Airport is the 235 acre wetlands of Kanaha Pond State Wildlife Sanctuary managed by the state of Hawaiʻi Department of Natural Resources, and owned by the Department of Transportation (i.e., Kahului Airport). Kanaha Pond State Wildlife Sanctuary was designated a National Natural Landmark in 1971 and serves as a wildlife refuge for endangered Hawaiian water bird species such as the aeʻo (Hawaiian stilt), koloa maoli (Hawaiian duck) and the ʻalae keʻokeʻo (Hawaiian coot). It consists of four land cover classifications: open water, palustrine emergent wetland, palustrine scrub shrub wetland, and palustrine forested wetland. Fluctuations in groundwater in Kahului correlate highly with fluctuations in local sea level (Rotzoll and El-Kadi 2008). Land elevation ranges from 0 to 30 m above local Mean Higher High Water (MHHW), with a mean elevation <6 m, as identified from the tidally adjusted LiDAR DEM. As a result, Kahului makes a prime location for SLR vulnerability mapping studies.
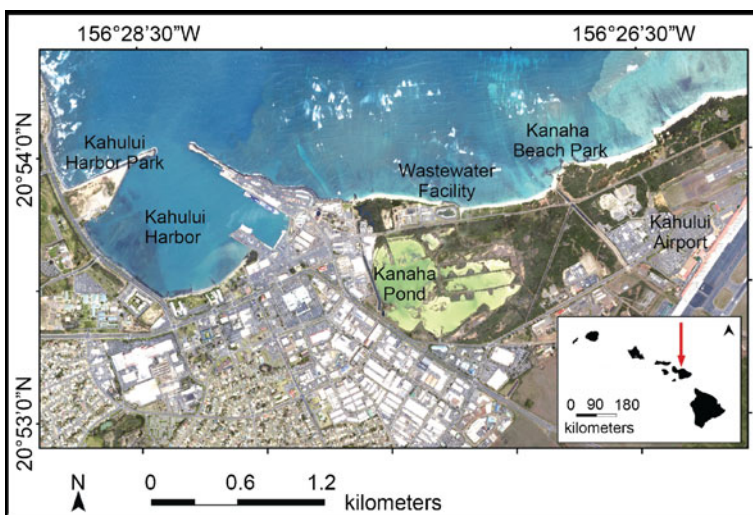


Fig. 1 Location of study area Kahului, Maui, and the main Hawaiian Islands chain

2.2 LiDAR data

The current best-available LiDAR data for Kahului is 2007 United States Army Corps of Engineers (USACE) LiDAR. USACE contracted Joint Airborne LiDAR Bathymetry Technical Center of Expertise (JALBTCX) for airborne topographic LiDAR data collection along the northern coast of Maui from 11 through 27 January 2007 using an Optech Inc., SHOALS-3000 instrument. The vendor post-processed the LiDAR data using TerraScan software, and the delivered product was a file of xyz points defined in a coordinate system designated as either "unclassified state" or "ground." The nominal post-spacing quoted is approximately 1.3 m between points. The vendor tested the LiDAR return file against ground truth data using post-processed kinematic GPS with a horizontal error of ±0.75 m (1 σ) and vertical error of ±0.20 m (1 σ). Since no information on the data distribution is provided for Monte Carlo simulation, we consider the quoted vertical error of 0.20 m (σ) and assume a Gaussian distribution and that the data provider followed NSSDA (FGDC 1998) guidelines. Toolbox for LiDAR Data Filtering and Forest Studies (Tiffs) software (Chen 2007) uses a morphological method for filtering LiDAR ground returns, which was implemented for refining the filtering results from TerraScan to extract ground points using the filtering parameters: a) there are at least 2 ground points within 20 m, b) ground points are less than 0.2 m above ground, and c) minimum ridge slope is 0.1°, before generating a 2 m LiDAR DEM.

3 Methods

Here, we provide an overview of our methods. The LiDAR is transformed from Mean Sea Level (MSL) to MHHW using tidal benchmarks and local water levels at the Kahului Harbor tide station for a tidally adjusted DEM. It is not common practice to complete a formal probability analysis on SLR projections, so we utilize the approach by Purvis et al. (2008) to formalizing the unknown real distribution of SLR estimates in terms of a triangular distribution. Monte Carlo simulation is used to propagate LiDAR, transformation and SLR estimates probability distributions through our inundation model. The output probability rasters are generalized as areas of high and low probability of inundation, which are used to determine the effect of combining uncertainties on assessing vulnerable land area and land cover for Kahului, Maui.

3.1 Local water levels

No conversion between orthometric and tidal datums is necessary for the LiDAR. This is because there is currently no accepted orthometric datum for the state of Hawai'i (such as NAVD 88 for the contiguous U.S.). NOAA and NGS are in charge of orthometric datums in the U.S. and its territories, and Hawaiian Islands vertical datum is a work in progress (National Geodetic Survey NGS 2012). Until then, LiDAR are vertically referenced to local MSL defined by the primary tide station on the respective Hawaiian Island.

   Local water level heights are used to measure vertical datums also known as tidal datums. In the U.S. and related territories, water level observations are collected and distributed by National Ocean Service (NOS) Center for Operational Oceanographic Products and Services (CO-OPS; http://tidesandcurrents.noaa.gov/). Tidal datums such as MSL and MHHW are defined by a certain phase of the tide at a fixed tide station location (National Oceanic Atmospheric Administration NOAA 2003). MSL is the average of the mean sea level

heights of each tidal day (collected in 6-minute intervals), and MHHW is the average of the mean higher high water heights of each tidal day (collected in 6-minute intervals), both observed over a National Tidal Datum Epoch (NTDE) of 19 years (National Oceanic Atmospheric Administration NOAA 2003). A series length of 19 years is chosen because it has astronomic significance (it considers the 18.61 year lunar cycle; Hicks 2006). It is important to note that non-astronomical short-term changes such as wave setup and coastal-trapped eddy waves may not be as significant over a 19 year average as are longer-term oscillations such as southern oscillation and pacific decadal oscillation. However, the amount of variability in this time span that is affected by these longer-term changes is not considered. The current NTDE is 1983 through 2001, with local MSL value of 1.075 m above Station Datum, and MHHW value of 1.422 m above Station Datum observed at the Kahului Harbor tide station. The Station Datum is defined as a fixed base established at an elevation below the water that is used for referencing tidal datums (http://tidesandcurrents.noaa.gov/; also see Fig. 3 in Cooper et al. 2013). Hence, local water levels averaged as a tidal datum serve as an important vertical reference system.

The LiDAR is vertically referenced to MSL tidal datum, but it is unclear to which tidal datum epoch. We assume best practices by the LiDAR provider is to reference the data to MSL for a series length of 19 years that agrees with the time of data collection, and not the current NTDE of 1983 through 2001. A transformation from MSL to MHHW is necessary because we are mapping future SLR above the highest watermark where land is inundated daily. Therefore, monthly averages of verified water levels of MSL and MHHW are obtained for Kahului Harbor tide station from January 1988 through December 2006 from NOS CO-OPS to match the time of LiDAR data collection. Then we compute the average of the MSL elevations of each month to define MSL (1988–2006 epoch; Table 1). Since the LiDAR is tested against tidal benchmarks referenced to MSL 1983–2001 epoch to calculate a mean vertical error (i.e., bias of 9 cm; Cooper et al. 2012), this bias needs to be adjusted to the MSL 1988–2006 epoch. Therefore, the difference between MSL 1988–2006 epoch (1.09 m) and MSL 1983–2001 epoch (1.075 m) of 1.5 cm is used to adjust the 9 cm mean vertical error to 7.5 cm. As a result, the LiDAR is decreased by 7.5 cm to correct for this bias. The MSL 1988–2006 epoch constant is also used to compute the standard deviation (0.06 m) and mean difference (0.35 m) between varying monthly MHHW from 1988 to 2006 (Table 1), and we infer a Gaussian distribution from an observed frequency distribution. The LiDAR values are then decreased by the mean difference (0.35 m). Accordingly, the LiDAR is transformed from MSL to MHHW 1988–2006 epoch for a tidally adjusted LiDAR DEM.

**Table 1** Descriptive statistics for verified monthly water levels observed over 19 years from January 1988 through December 2006 at the Kahului Harbor tide station on Maui Island. Where MSL=Mean Sea Level, MHHW=Mean Higher high water, μ=mean, n=the number of monthly observations, σ=standard deviation, $\Delta_{MHHW}$=the difference between monthly MHHW observations and 19 year MSL. Data downloaded from http://tidesandcurrents.noaa.gov/

| Tidal datum (1988–2006) | μ (m) | Median (m) | Skew | σ (m) | n | Minimum (m) | Maximum (m) |
|---|---|---|---|---|---|---|---|
| MSL | 1.09 | 1.09 | 0.07 | 0.0568 | 228 | 0.95 | 1.27 |
| MHHW | 1.44 | 1.44 | −0.12 | 0.0600 | | 1.29 | 1.59 |
| $\Delta_{MHHW}$ | 0.35 | 0.35 | −0.12 | 0.0600 | | 0.20 | 0.50 |

3.2 Formalizing SLR estimates

Stating SLR estimates as a probability distribution is necessary to account for the uncertainty in the range of those estimates. The current MSL trend for Kahului (2.32±0.53 mm/year; http://tidesandcurrents.noaa.gov/sltrends/) is less than the global average (3.2±0.4 mm/year; Church and White 2011). While regional SLR estimates and their timing are ideal for coastal inundation mapping, there are currently no comprehensive assessments for Hawaiian coasts. Therefore, we consider recent global SLR estimates identified by Schaeffer et al. (2012) using the Representative Concentration Pathway (RCP) 4.5. Schaeffer et al. (2012) estimate global SLR in the range of 0.64–1.21 m with a central median value of 0.9 m by year 2100 (relative to 2000 levels) using the RCP4.5 scenario. Although there is no evidence of skewed data, there is also no information provided on the mean, standard deviation, and frequency distribution of these estimates to assume symmetry. We proceed by approximating the unknown real distribution (e.g. whether it is Gaussian, non-Gaussian, uniform, etc.) as a triangular distribution closely following Purvis et al. (2008). A probability of 0 is assigned to any SLR values below 0.64 or above 1.21 m (assuming the best-case scenario where ice sheet collapse does not exceed a SLR of 1.21 m by 2100). Then a probability of 0.5 is assigned to the ranges 0.64–0.9 m and 0.9–1.21 m, respectively. This allows us to state a probability of 1 for SLR between 0.64 and 1.21 m by 2100. It follows that the probability of SLR ($P_{SLR}$) in meters is given using the following equation:

$$
\begin{aligned}
&P_{SLR} \,|\, SLR < 0.64 = 0 \\
&P_{SLR} \,|\, SLR > 1.21 = 0 \\
&\sum_{P_{SLR}=0.64}^{0.9} P_{SLR} = \sum_{P_{SLR}=0.9}^{1.21} P_{SLR} = 0.5 \\
&\sum_{P_{SLR}=0.64}^{1.21} P_{SLR} = 1
\end{aligned}
\tag{1}
$$

It is also reasonable given the information provided on the range and median, although not absolutely necessary, that the median of 0.9 m is likely correct. Thus, we arrive at a triangular function as the most basic probability distribution that fits these data (Fig. 2). As a result, the future SLR estimates are formalized as a probability distribution so that we may consider their uncertainty in the vulnerability mapping.
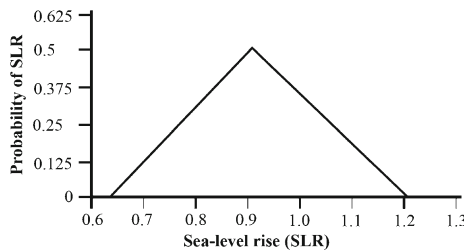


Fig. 2 Probability distribution for sea-level rise by 2100 derived using Purvis et al. (2008) approach to formalizing RCP4.5 scenario estimates by Schaeffer et al. (2012). Sea-level rise values are in meters

### 3.3 Mapping coastal inundation

Two approaches are used for mapping coastal inundation. First, all grid cells in the LiDAR DEM with elevations below the SLR median of 0.9 m hydrologically and not hydrologically connected with the ocean and wetland are identified to produce a raster that considers no uncertainty. Second, uncertainty is considered using Monte Carlo technique to propagate probability distributions through our probability inundation model. The following equation is used to consider LiDAR and transformation uncertainty:

$$P_{x,y} = \sum \left( \sigma_{\Delta_{MHHW}} + SLR > LiDAR + LiDAR_{x,y} \right) \qquad (3)$$

where $P_{x,y}$ is the probability of a grid cell at $x,y$ location of being inundated taking a value anywhere from 0 to 1, $\sigma_{\Delta_{MHHW}}$ is a random variable sampled from Gaussian distribution (0, 0.06), $SLR$ is the constant median of 0.9 m, $LiDAR$ is a random variable sampled from Gaussian distribution (0, 0.2), and $LiDAR_{x,y}$ is a constant elevation value of a grid cell at $x,y$ location all in meters. The following equation is used to consider LiDAR, transformation and SLR estimates uncertainty:

$$P_{x,y} = \sum \left( \sigma_{\Delta_{MHHW}} + SLR_r > LiDAR + LiDAR_{x,y} \right) \qquad (4)$$

where the only difference from Eq. 3 is that $SLR_r$ is a random variable sampled from a triangle distribution with a range between 0.64 and 1.21 and most probable value (0.9). The sampling procedure for both Eqs. 3 and 4 is repeated 10,000 times for each grid cell. The outputs are a new 2 m resolution raster where each grid cell contains a probability value anywhere between 0 and 1 of being inundated.

### 3.4 Assessing vulnerable land area

The rasters that consider 1) no uncertainty, 2) uncertainty in LiDAR and transformation, and 3) uncertainty in LiDAR, transformation and SLR estimates are used to calculate vulnerable land area. The raster that considers no uncertainty is converted to a polygon layer. The two probability rasters are generalized using a ranking scheme similar to National Oceanic Atmospheric Administration (NOAA) (2010). The probability rasters are reclassified by assigning the range of probability values 0–0.19 equal to 0, 0.19–0.79 equal to 20 (low probability), and 0.79–1 equal to 80 (high probability). The two generalized probability rasters are used to produce four generalized polygon layers that 1) include uncertainty in LiDAR and transformation at either the high or low probability thresholds, and 2) include uncertainty in LiDAR, transformation and SLR estimates at either the high or low probability thresholds. As in NOAA's Coastal Services Center (CSC) SLR mapping visualization tool (http://www.csc.noaa.gov/slr/viewer), we do not distinguish submerged areas hydrologically connected with the ocean differently from areas not hydrologically connected with the ocean. The polygon layer that considers no uncertainty and the four generalized probability layers are then used to calculate total land area vulnerable to potential inundation. Therefore, the effect of uncertainty on land area inundated can be assessed.

### 3.5 Assessing vulnerable land cover

The generalized probability layers at either the high or low probability thresholds that 1) include uncertainty in LiDAR and transformation, and 2) include uncertainty in LiDAR,

transformation and SLR estimates are used together with high resolution land cover data to determine the effect of these uncertainties combined on probable land cover loss. NOAA CSC Coastal Change Analysis Program (C-CAP) land cover was derived for Maui Island by delineating high resolution Quickbird multispectral scenes collected 20 November 2005. The C-CAP land cover layer is converted to polygon and intersected with the generalized probability layers to calculate the area. For each of the high and low probability thresholds, the difference between the area of a land cover classification inundated when considering uncertainty in 1) LiDAR and transformation, and 2) LiDAR, transformation and SLR estimates is calculated. As a result, we can evaluate the effect of combining these uncertainties on estimating potential land cover loss.

## 4 Results and discussion

### 4.1 Difference in probability

A difference grid was generated by reducing the probability raster that includes 1) uncertainty in LiDAR, transformation and SLR estimates by the probability raster that 2) includes uncertainty in LiDAR and transformation to examine the impact of including uncertainty in SLR estimates on identifying a grid cell's probability being inundated. The difference is shown in Fig. 3a, b. It follows that the difference in the probability of potential inundation between the
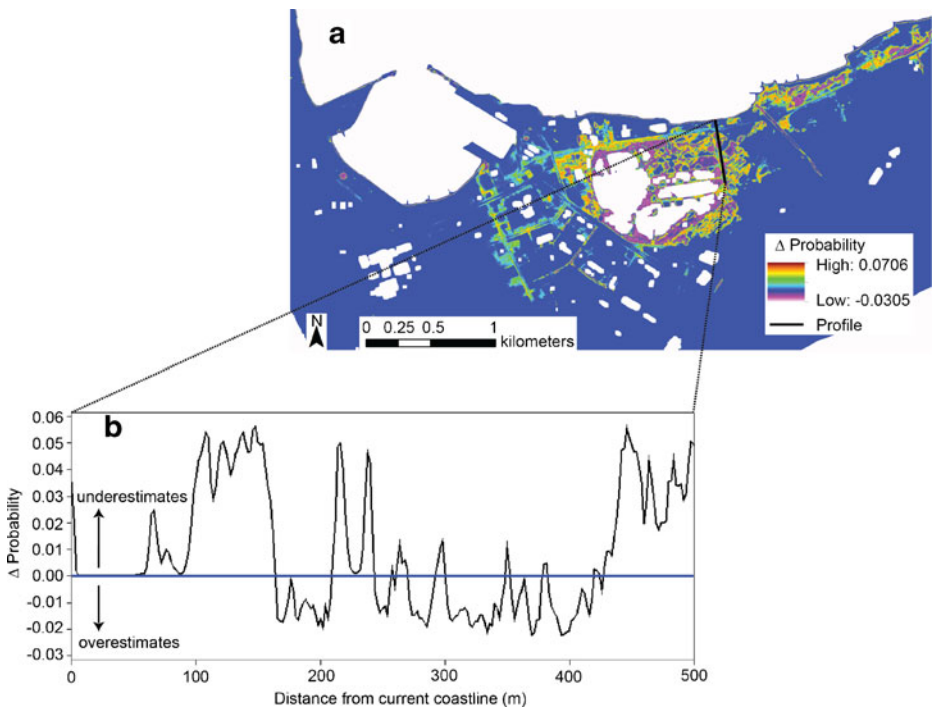


**Fig. 3** Difference (Δ) between the probability raster that considers uncertainty in LiDAR, transformation and sea-level rise (SLR) estimates, and probability raster that considers uncertainty in LiDAR and transformation (**a**). The Δ probability profile through Kanaha Pond State Wildlife Sanctuary demonstrates areas either over or underestimated when we do not consider uncertainty in SLR estimates (**b**)

two rasters ranges 10 % (see Fig. 3a). In particular, the difference in the probability profile through Kanaha Pond State Wildlife Sanctuary (Fig. 3b) demonstrates areas that are either under or overestimated when we do not consider uncertainty in future SLR estimates. These results show that the probability of a grid cell being inundated in the raster that considers uncertainty in just LiDAR and transformation varies in over and underestimating potential inundation.

4.2 Effect of uncertainty on land area

The land area vulnerable to potential inundation under the three cases is summarized in Table 2. The sum of vulnerable land area is consistently understated when considering no uncertainty. It results that there is a −32.2 % difference in land area inundated when compared to considering uncertainty in LiDAR and transformation, and a −40.4 % difference in land area inundated when compared to considering uncertainty in LiDAR, transformation and SLR estimates. The sum of vulnerable land area for both the high and low probability thresholds shown in Table 2 is also understated by −6.8 % when considering uncertainty in LiDAR and transformation alone. Additionally, considering uncertainty in just LiDAR and transformation overestimates land area by +2.6 % for the high probability threshold, and understates vulnerable land area by −14.1 % for the low probability threshold.

Using the confidence interval approach to mapping coastal inundation uncertainty by Gesch (2013), the vulnerable land area should be reported as a range and not a single number. Our Monte Carlo approach suggests that vulnerable land area can also be reported as a single number while considering uncertainty (Table 2). Furthermore, previous studies show that not considering uncertainty in LiDAR (Gesch 2009) or future SLR estimates (Purvis et al. 2008) underestimates the sum of vulnerable land area. Our results show that the sum of vulnerable land area for both the high and low probability thresholds is also understated when considering uncertainty in just LIDAR and transformation. However, considering uncertainty in just LiDAR and transformation can either under or overestimate vulnerable land area depending on how the high and low probability thresholds are defined. If lands vulnerable at the high probability threshold are considered first priority for adaptation measures, then decision makers who utilize these assessments that ignore uncertainty in SLR estimates will make conservative decisions for Kahului because vulnerable land area is slightly overestimated. On the other hand, lands vulnerable at the low probability threshold may be considered second priority for adaptation decisions, and decision makers who utilize these assessments that ignore uncertainty in SLR estimates will make less reliable decisions for Kahului because vulnerable land area is underestimated. This suggests that considering uncertainty in future SLR estimates is essential when defining the sum of vulnerable land area, and when defining areas vulnerable at the low probability threshold, at least in our study area.

**Table 2** The effect of a) no uncertainty, b) uncertainty in LiDAR DEM and transformation, and c) uncertainty in LiDAR DEM, transformation and SLR estimates on total land area inundated. Where Σ=sum

| Probability | No uncertainty (area km²) | Uncertainty in LiDAR DEM and transformation (area km²) | Uncertainty in LiDAR DEM, transformation and SLR estimates (area km²) |
|---|---|---|---|
| High | | 0.268 | 0.261 |
| Low | | 0.316 | 0.364 |
| Σ | 0.422 | 0.584 | 0.625 |

4.3 Effect of uncertainty on land cover

The difference in area of a land cover category potentially inundated at each of the high and low probability thresholds when considering uncertainty in 1) LiDAR and transformation, and 2) LiDAR, transformation and SLR estimates is shown in Fig. 4. In exception to no difference in cultivated land cover when considering uncertainty in just LiDAR and transformation at the high probability threshold, the percentage within all other land cover classifications is consistently overestimated in a range from 0.4 % to 29.9 %. On the other hand, considering uncertainty in just LiDAR and transformation at the low probability threshold consistently underestimates the percentage within all land cover classifications where cultivated and estuarine forest wetland land cover differences are small (0.03 % and 0.06 %), and all other land covers are underestimated in a range from 4 % to 27 %.

One study uses LiDAR to examine the effect of inundation on land cover (Chust et al. 2010), while few studies examine the effect of inundation on land cover while considering uncertainty in LiDAR (Gesch 2009), and LiDAR and transformation (Gesch 2013). Here, we apply possible adaptation approaches from Nichols (2011) in the case of our study area while considering the effects of including uncertainty in just LiDAR and transformation compared to considering uncertainty in LiDAR, transformation and SLR estimates. Kanaha Beach Park is categorized as bare land, and Maui planners who favor soft approaches of coastal protection such as replenishment may be relieved that bare land is overstated by only 2.7 % of all vulnerable land covers at the high probability threshold, thus allowing for more conservative adaptation decisions if uncertainty in SLR estimates is not considered. Maui urban planners are
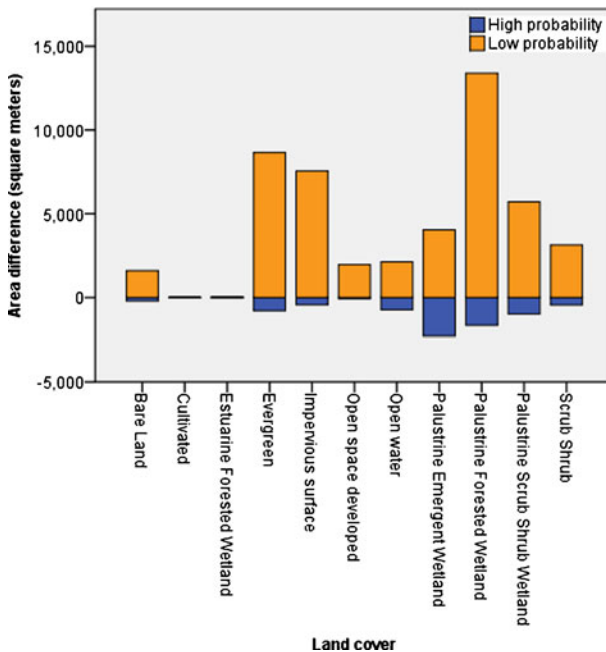


Fig. 4 Difference (Δ) in land cover between considering uncertainty in 1) LiDAR, transformation and SLR estimates, and 2) LiDAR and transformation for each of the high and low probability thresholds. Where excluding uncertainty in SLR estimates consistently overestimates land cover at the high probability threshold, and consistently underestimates land cover at the low probability threshold

likely most concerned with impervious surface and open space developed land covers that together are overestimated by 6.8 % of all vulnerable land covers at the high probability threshold, and underestimated by 19.7 % of all vulnerable land covers at the low probability threshold. Thus, uncertainty in SLR estimates should be included in the vulnerability assessments so that effective decisions of hard approaches such as drainage systems, and as in the case of Kahului Harbor, accommodation and retreat approaches such as land-use planning and hazard delineation are implemented. The majority of inundated land cover categories are the four types that make up Kanaha Pond State Wildlife Sanctuary (see section 2.1), which is a natural reclamation of water areas. These land covers altogether are underestimated by 52 % of all vulnerable land covers at the low probability threshold, and overestimated by 65.6 % of all vulnerable land covers at the high probability threshold. Thus, uncertainty in SLR estimates should be included so that Managers at the state of Hawai'i Department of Natural Resources can more effectively consider migration space for wetland expansion and accommodation and retreat approaches such as land-use planning. This suggests that not considering uncertainty in future SLR estimates in addition to LiDAR and transformation has variable effect on SLR adaptation decisions depending on the land cover category and how the high and low probability thresholds are defined.

## 5 Conclusion

The obejectives of this paper are: 1) evaluate the effect of combining uncertainties in LiDAR, transformation and future SLR estimates on estimating potential land area and land cover loss, and 3) examine whether including uncertainty in future SLR has implications for adaptation decisions in Kahului, Maui. We use a Monte Carlo approach to produce probability rasters that are generalized to a high (cells between 80th and 100th percentile) or low (cells between 20th and 80th percentile) probability of being inundated. We identify the following:

- The probability of inundation generated by ignoring uncertainty in SLR estimates differs from that produced by considering uncertainty in SLR estimates with a range of 10 %.
- Assessments that ignore uncertainty in SLR estimates at the high probability threshold will result in conservative adaptation decisions for Kahului because land area is overestimated by 2.6 %. Assessments that ignore uncertainty in SLR estimates at the low probability threshold will result in less reliable adaptation decisions for Kahului because land area is underestimated by 14.1 %.
- Maui planners will want to consider uncertainty in SLR estimates for open space developed and impervious surface land covers, especially at Kahului Harbor, so that reliable approaches such as drainage systems, land-use planning and hazard delineation are implemented.
- It is essential to consider uncertainty in SLR estimates when calculating vulnerable land covers within Kanaha Pond State Wildlife Sanctuary, so that managers can take the right course of action when considering migration space for wetland expansion and land-use planning.
- Not considering uncertainty in future SLR estimates has variable effect on SLR adaptation decisions depending on the land cover category and how the high and low probability thresholds are defined.
- SLR vulnerability assessments will benefit if future studies of SLR projections and LiDAR data providers make available information on the distributions so that researchers can utilize the appropriate approach to considering uncertainty in SLR vulnerability assessments.

It is expected that this paper will help improve mapping SLR vulnerability and assessments. The authors identify continuing research in areas of incorporating uncertainties into modeling other physical effects of SLR such as increased storm surges (e.g., Zhang et al. 2013), wave setup (e.g., Reynolds et al. 2012), and groundwater inundation (e.g., Rotzoll and Fletcher 2012). As we begin to better understand and quantify other uncertainties due to the physical effects of future SLR, using randomization to represent distributions is a valuable approach to addressing uncertainty when errors do not follow a Gaussian distribution.

# References

Chen Q (2007) Airborne LiDAR data processing and information extraction. Photogram Eng Rem S 73:109–112

Church J, White N (2011) Sea-level rise from the late 19th to the early 21st century. Surv Geophys 32:585–602

Chust G, Caballero A, Marcos M, Liria P, Hernandez C, Borja A (2010) Regional scenarios of sea-level rise and impacts on Basque (Bay of Biscay) coastal habitats, throughout the 21st century. Estuar Coast Shelf Sci 87(1):113–124

Cooper H, Chen Q, Fletcher C, Barbee M (2012) Vulnerability assessment due to sea-level rise in Maui, Hawai'i using LiDAR remote sensing and GIS. Clim Chang 116:547–563

Cooper H, Fletcher C, Chen Q, Barbee M (2013) Sea-level rise vulnerability mapping for adaptation decisions using LiDAR DEMs. Prog Phys Geog. doi:10.1177/0309133313496835

FGDC (1998) Geospatial positioning accuracy standards, Part 3. National Standard for Spatial Data Accuracy. FGDC-STD-007.3-1998  http://www.fgdc.gov/standards/projects/FGDCstandardsprojects/accuracy/part3/index_html. Accessed 10 November 2012.

Gesch D (2009) Analysis of Lidar elevation data for improved identification and delineation of lands vulnerable to sea-level rise. J Coastal Res 53:49–58

Gesch D (2012) Elevation uncertainty in coastal inundation hazard assessments. In: Cheval S (ed) Natural Disasters: Rijeka. Croatia, InTech, pp 121–140

Gesch D (2013) Consideration of vertical uncertainty in elevation-based sea-level rise assessments: Mobile bay, Alabama case study. J Coastal Res 63:197–210

Hicks SD (2006) Understanding tides. http://tidesandcurrents.noaa.gov/publications/Understanding_Tides_by_Steacy_finalFINAL11_30.pdf. Assessed 20 December 2012.

JCGM, Joint Committee for Guides in Metrology (2008) JCGM 101:2008. Evaluation of measurement data – supplement 1 to the "Guide to the expression of uncertainty in measurement" - propagation of distributions using a Monte Carlo method. http://www.bipm.org/en/publications/guides/gum.html. Accessed 8 August 2013.

Meehl G, Stocker T, Collins W, Friedlingstein P, Gaye A, Gregory J, Kitoh A, Knutti R, Murphy J, Noda A (2007) Global Climate Projections. Chapter 10 in Climate Change 2007: The Physical Science Basis. In: Solomon S, Qin D, Manning M (eds) Contribution of working group I to the fourth assessment report of the intergovernmental panel on climate change. Cambridge University Press, Cambridge UK, and New York, NY

Mitsova D, Esnard A, Li Y (2012) Using dasymteric mapping techniques to improve the spatial accuracy of sea level rise vulnerability assessments. J Coast Conservat 16(3):355–372

National Geodetic Survey (NGS) (2012) Vertical Datums (available online at: http://www.ngs.noaa.gov/datums/vertical/VerticalDatums.shtml).

National Oceanic and Atmospheric Administration (NOAA) (2012) Estimation of vertical uncertainties in VDatum. Available at: http://vdatum.noaa.gov/docs/est_uncertainties.html.

National Oceanic Atmospheric Administration (NOAA) (2003) Computational techniques for tidal datums handbook. NOAA special publication NOS CO-OPS 2. NOAA National Ocean Service, Silver Spring, MD.

National Oceanic Atmospheric Administration (NOAA) (2010) Mapping Inundation Uncertainty.

Nichols RJ (2011) Planning for the impacts of sea level rise. Oceanography 24(2):144–157

NOAA Coastal Services Center http://www.csc.noaa.gov/beta/slr/assets/pdfs/Elevation_Mapping_Confidence_Methods.pdf. Assessed 2 June 2012.

Poulter B, Halpin P (2008) Raster modeling of coastal flooding from sea-level rise. Int J Geogr Inf Sci 22(2):168–182

Purvis M, Bates P, Hayes C (2008) A probabilistic methodology to estimate future coastal flood risk due to sea level rise. Coast Eng 55(12):1062–1073

Reynolds M, Berkowitz P, Courtot KN, Krause C, eds. (2012) Predicting sea-level rise vulnerability of terrestrial habitat and wildlife of the Northwestern Hawiian Islands: U.S. Geological Survey Open-File Report 2012–1182, 139 p.

Rotzoll K, El-Kadi AL (2008) Estimating hydraulic properties of coastal aquifers using wave setup. J Hydrol 353:201–213

Rotzoll K, Fletcher C (2012) Assessment of groundwater inundation as a consequence of sea-level rise. Nature Clim Change 3:477–481

Schaeffer M, Hare W, Rahmstorf S, Vermeer M (2012) Long-term sea-level rise implied by 1.5°C and 2°C warming levels. Nature Clim Change 2:867–870

U.S. Climate Change Science Program (2009) Synthesis and assessment product 4.1 Coastal sensitivity to sea-level rise: a focus on the mid-Atlantic region. U.S. Environmental Protection Agency, Washington, DC, p 320

Zhang K (2011) Analysis of non-linear inundation from sea-level rise using LiDAR data: A case study for South Florida. Clim Chang 106(4):537–565

Zhang K, Li Y, Liu H, Xu H, Shen J (2013) Comparison of three methods to estimate the sea level rise effect on storm surge flooding. Clim Chang 118(2):487–500